ISSN 2079-0864, Biology Bulletin Reviews, 2018, Vol. 8, No. 1, pp. 23–31. © Pleiades Publishing, Ltd., 2018.
Original Russian Text © A.V. Romashchenko, D.V. Petrovsky, M.P. Moshkin, 2017, published in Zhurnal Obshchei Biologii, 2017, Vol. 78, No. 1, pp. 15–24.

Congruence of Intranasal Aerodynamics and Functional Heterogeneity of Olfactory Epithelium

A. V. Romashchenko[a, b], D. V. Petrovsky[a], and M. P. Moshkin[a, c, *]

[a] *Institute of Cytology and Genetics, Siberian Branch, Russian Academy of Sciences, Novosibirsk, 630090 Russia*
[b] *Design Technological Institute of Digital Techniques, Siberian Branch, Russian Academy of Sciences, Novosibirsk, 630090 Russia*
[c] *Tomsk State University, Tomsk, 634050 Russia*
**e-mail: mmp@bionet.nsc.ru*

Received May 31, 2016

Abstract—Zonal organization of the olfactory system is determined not only by peculiarities of the expression of olfactory receptor genes but also by the geometry of nasal passage, where receptors to the most muco-soluble compounds are concentrated in the area with the maximal rate of air flow (dorsal part), while receptors to less volatile compounds are concentrated in ventral part of the nose. An increase in the flow rate in certain areas of nasal cavity, on the one hand, allows acceleration of the perception of odor stimuli by olfactory receptors and, on the other hand, increases the risk of the effect of different pathogens (contained in the air) on this area due to the larger intensity of their precipitation. In this study, we demonstrated by means of manganese-enhanced magnetic resonance imaging (MRI) that a more intensive capture of insoluble particles occurs in ventral part of mouse olfactory epithelium than in dorsal part during intranasal introduction of the colloid solution of manganese oxide nanoparticles (MON, Mn_3O_4). The joint introduction of MON and specific blockers of cellular transport and endocytosis demonstrated that the particles are captured from the nasal cavity by means of endocytosis and are transported in olfactory bulb cells by means of intracellular transport. The clathrin-dependent type of endocytosis mainly contributes to the capture of MON in the dorsal part of the olfactory epithelium (as opposed to ventral). Thus, it was established that two functional regions of mouse olfactory epithelium differing in the intensities of precipitation of submicron aerosols demonstrate different intensities of the capture of insoluble particles from the nasal cavity and have differences in the mechanisms of their endocytosis. Consequently, the structural and functional organization of mouse nasal cavity completely meets the principle of adaptive congruence, which limits infectious and toxic effects of nanoaerosols on the olfactory epithelium cells and the brain.

DOI: 10.1134/S207908641801005X

INTRODUCTION

In the process of life, the organism is constantly exposed to the effect of different pathogens: viruses, bacteria, fungal spores, and soluble and insoluble forms of xenobiotics. In the composition of aerosols, the pathogens settle on the mucous membranes of upper and lower respiratory tract and are able to penetrate into the organism circulatory system and accumulate in internal organs. Their penetration from the blood to CNS is complicated by the blood–brain (BBB) and blood–cerebrospinal fluid barriers. The possibility of transport directly from nasal cavity to the brain bypassing the BBB was demonstrated for a number of pathogens. The first evidence of direct supply of nanoaerosols from the nasal cavity to the brain were obtained in experiments with intranasal infection of monkeys with poliomyelitis virus. The destruction of olfactory epithelium by zinc sulfate prevented viral penetration of the brain (Faber et al., 1944). Not only viruses (the sizes of which vary from 30 to 300 nm) but some bacteria (for example, the *Burkholderia pseudomallei* (2000–5000 nm) and *Streptococcus pneumonia* (500–1250 nm)) penetrated from the nasal cavity into different brain structures. Their presence in the blood was not detected (John et al., 2014; Dando et al., 2014). It was demonstrated in a number of works that the intranasal application of manganese, titanium, and silicon oxide nanoparticles to mice and rats also leads to their accumulation in the brain, primarily in the olfactory bulbs (Oberdorster et al., 2004; Elder et al., 2006; Wang et al., 2008; Wu et al., 2011). It was also noted that the inhalation of nanosized aerosol of manganese oxide in animals with the occlusion of one nostril is accompanied by a significant increase in the concentration of a metal in the olfactory bulb located ipsilateral relative to the open nasal passage. The Mn content in the contralateral bulb remains at the control level (Elder et al., 2006). The possibility of the transport of solid particles from nasal cavity to the brain

raises a question about the role of this process in the development of different neurodegenerative diseases.

A number of peculiarities were detected in the comparison of the toxicity of soluble and insoluble forms of xenobiotics. It was demonstrated on A549 cell culture that superparamagnetic ferrum particles are able to cause single-stranded DNA breaks. The toxicity of solid particles can be also manifested in the fact that, with penetration of the cell by means of endocytosis, they can be exposed to partial dissolution and thus create a higher local concentration of ions (Chattopadhyay et al., 2015). In addition, it was demonstrated in a study conducted on PC-12 cell culture that both manganese oxide (40 nm) and manganese chloride(II) decrease the concentration of dopamine and its metabolite, while the concentration of free radicals is five times higher during the addition of manganese oxide in the culture as compared with a similar dose of $MnCl_2$ (Hussain et al., 2006). Thus, the penetration by solid particles of bacterial, viral, and nonorganic natures from the nasal cavity to the brain can provoke the development of different neurological disorders. Thus, a violation in the perception of olfactory stimuli is one of the first symptoms of the development of a number of dementia (Parkinson's disease, Alzheimer's disease); therefore, the effects of environmental factors, including the components of inhalable aerosols, are considered possible ecological risk factors for these diseases (Calderón-Garcidueñas et al., 2013).

Based on the above, the existence of the animals under conditions of a high concentration of nanoaerosols raises a question about the mechanisms limiting the supply of potential pathogens from the nasal cavity to the brain. One of the first pieces of evidence of adaptive response to the habitation in the environment saturated with submicron and nanosized powder was obtained during a comparative study of the geometry and aerodynamics of nasal passages in typical members of underground (northern mole vole) and ground (house mouse) rodent species (Moshkin et al., 2015). As is known, northern mole voles feed on the plant roots, access to which is obtained due to the digging of multimeter tunnels. They dig with their incisors; in dry soil, this leads to an inevitable saturation of inhalable air by dust particles of different sizes. Numerical simulation of the precipitation of micro- and nanosized aerosols demonstrated that sedimentation of model particles (sizes <100 nm) on the olfactory epithelium surface is almost six times lower in the burrowing rodent as compared with the ground rodent (Moshkin et al., 2014). Accordingly, it is possible to expect a smaller supply of nanoparticles in the brain of northern mole vole than in the house mouse during the inhalation of aerosols. This assumption was checked in an experiment with exposure of the compared species in an atmosphere containing magneto-contrast nanoaerosols. After a 3-h stay in an environment saturated with nanosized aerosols, a weaker intensity of T1-weighted images of magnetic resonance imaging (MRI) was registered in the burrowing species as compared with those in the ground species.

Numerical simulation of air flows in animal and human noses predicts a heterogeneous accumulation of nanoaerosols in different nasal cavity regions (Shi et al., 2008; Garcia and Kimbell, 2009; Garcia et al., 2015). In particular, the rate of air flows and, as a consequence, the intensity of nanoparticle precipitation in house mice is higher in the dorsal region of olfactory epithelium (OE) as compared with the ventral (Moshkin et al., 2014). This leads to a faster supply of organic volatile compounds (of both signal and toxic character) in this area, as well as to larger precipitation of nanosized particles on the surface of dorsal OE (Moshkin et al., 2014; Jiang et al., 2010).

There are three possible ways of penetration of solid nanosized aerosols from the nasal cavity to the brain: axonal (the capture by olfactory receptor neurons and trigeminal nerve ends), para-cellular (by intercellular space along axons), lymphatic (lymphatic vessels of nasal cavity, passing through the trellised bone, fall into subarachnoid space). Direct evidence of the pathogen penetration from the nose to the brain by means of axonal transport were obtained by means of immunohistochemistry for Nipah virus (Munster et al., 2012), the *Burkholderia pseudomallei* bacteria (John et al., 2014), and fluorescent nanocrystals Qdots (Hopkins et al., 2014). During a study of the supply of intranasally introduced viral particles of Sendai and Venezuelan equine encephalitis to the brain, their accumulation in the olfactory epithelium and olfactory bulbs was established (Mori et al., 1995, 2005; Ryzhikov et al., 1995). Very little is known about the mechanisms of the capture of solid particles by olfactory epithelium. Since solid particles cannot enter the cell directly through ion channels, endocytosis (the mechanisms of which can be not the same in different nose regions) is the most probable penetration mechanism.

Thus, a question arises about the mutual correspondence of morphofunctional heterogeneity of OE and heterogeneous precipitation of aerosols on the OE surface (caused by the nose geometry). In this work, we used manganese oxide nanoparticles (MON, Mn_3O_4) to analyze the efficiency of the capture and transport of solid particles by olfactory neurons located in different regions of mouse nasal cavity. Since manganese reduces the time of proton T1 relaxation and thus gives a positive (white) signal during MRI, the accumulation of MON in the olfactory epithelium (OE) and olfactory bulb (OB) was determined by manganese-enhanced MRI. In order to exclude the effect of the nose geometry on the capture of particles, the colloid MON solution was introduced in an excess volume intranasally, and the accumulation of particles in OB and OE was estimated 12 h after introduction; based on preliminary experiments, this corresponds to the time at which the MON concentration in OB is

maximal. This parameter makes it possible to estimate most adequately the intensity of the capture of OE particles. To detect the reasons for the differing efficiency of the supply of nanoparticles in the brain from different regions of nasal cavity, intranasal introduction of MON was combined with the preliminary introduction of specific and nonspecific inhibitors of the cellular transport and endocytosis. In addition, a comparative analysis of manganese accumulation in different OB regions during the introduction of Mn^{2+} ions (that penetrate into olfactory neurons through calcium channels) in the nasal cavity was conducted.

MATERIALS AND METHODS

Preparation of Manganese Oxide(II) Nanoparticles

Commercial Mn_3O_4 nanoparticles (US Nano, the United States) were used. According to the manufacturer's passport characteristics, they had a size of 30 nm and a surface area of 0.78 g/cm^3. One hour before introduction, MON were dispersed on an ultrasound QSonica Q700 homogenizer with a nonloaded probe (Cup Horn, QSonica, United States) at a frequency of 20 kHz and a power of 300 W/L. The sample was exposed to sonification for 30 one-minute cycles (30 with ON and 30 with OFF), and the MON parameters were then determined with Zetasizer NanoZS equipment (Malvern, England). The amplified particles had a hydrodynamic diameter of 135 ± 42 nm and a zeta potential of −28.0 ± 5.4.

Experimental Animals and Experiment Protocols

The work was conducted on the basis of the Center for Genetic Resources of Laboratory Animals of the Federal Research Center Institute of Cytology and Genetics, Siberian Branch, Russian Academy of Sciences (RFMEFI61914X0005 and RFMEFI62114X0010). The males of laboratory mice of the inbred C57Bl/6j line were studied at the age 12–14 weeks (28–32 g); after separation at the age 3 weeks, they were kept in groups of five individuals of the same sex in standard cages (35 × 25 × 12 cm) at a temperature of 22–24°C and an artificial light regime of 14L : 10D. Mice received the briquetted feed for laboratory rodents (SSNIFF-SPEZIALDIATENGMBH, Germany) and water ad libitum. Dust-free sawdust was used as a litter material.

$MnCl_2$ (0.1 M) and colloid magneto–contrast MON solutions were introduced intranasally in an excess volume by 8–10 μL in the right nostril. Since MRI changes caused by the introduction of manganese(II) ions or magneto–contrast manganese oxide particles were in linear dependence on the Mn concentration in biological tissues (Moshkin et al., 2014), the intensity of T1-weighted MRI images was used for semiquantitative estimation of the contents of MON and Mn^{2+}. The different durations of the presence of MON on the surface of OE was used to estimate the intensity of nanoparticle capture by the ends of olfactory nerves. For this purpose, the nasal cavity was washed by physiological solution (which was introduced once in a volume 50 μL) at different time intervals after intranasal MON introduction (10, 20, 40, 80, 120, and 180 min). Only 20 min of exposure, after which the introduced solution was washed away, was used in the experiments with $MnCl_2$ introduction. The groups for each time interval included five individuals. The accumulation of MON and Mn^{2+} (directly proportional to the intensity of MRI signal) was determined in the dorsal and central regions of OB 12 h after the application of nanoparticles. According to pilot experiments, the MRI signal level reaches peak values exactly at this time.

The effects of generally accepted endocytosis inhibitors and intracellular transport were studied to clarify the role of individual processes developing the movement of nanoparticles from the nasal cavity to the brain. Water solutions of inhibiting preparations were introduced in the right nostril (7 μL) 5 min before the application of MON. The inhibitors, their main effects, and references to the articles, in which the adequacy of used compounds for the purposes of our study is justified, are listed below:

—chlorpromazine (C8138, SIGMA, Sigma-Aldrich), specific inhibitor of clathrin-dependent endocytosis (Wang et al., 1993; Boucrot et al., 2015), the preparation was introduced at a dose of 0.1 mg/kg per mouse;

—saccharose (S0389 SIGMA, Sigma-Aldrich), nonspecific blocker of both clathrin-dependent and clathrin-independent endocytosis (Moore et al., 1995; Kittler et al., 2000), the preparation was introduced at a dose of 40 mg/kg per mouse;

—colchicines (C9754 SIGMA, Sigma-Aldrich), a compound suppressing tubulin polymerization, endocytosis, and cellular transport (Castel, 1990; Sloot and Gramsbergen, 1994), the preparation was introduced at a dose of 0.1 mg/kg per mouse.

An MRI study was conducted 12 h after the introduction of MON. Five individuals were studied in each experimental group, including five control animals that did not receive magneto-contrast compounds.

MRI

Mice were immobilized by a gas anesthesia (Isofluran, Baxter Healthcare Corp., United States) by means of an anesthesia machine (The Univentor 400 Anaesthesia Unit, Univentor, Malta) 5 min before the study. The animal temperature was supported by means of a water contour in tomography bed–table with a surface temperature of 30°C. A pneumatic breathing sensor (SA Instruments, Stony Brook, NY,

Table 1. Changes in the intensity of T1-weighted images in the ventral and dorsal OB upon the introduction of pharmacological inhibitors

Compound	Ventral OB, mean ± SE (n)	Dorsal OB, mean ± SE (n)	Significance of differences
Colchicine	$-88.59 \pm 3.08(5)^{a}$*	$-94.98 \pm 2.23(5)^{a}$	$t = 1.68$, $p = 0.13$
Saccharose	$-28.23 \pm 3.14(5)^{b}$	$-31.38 \pm 2.82(5)^{b}$	$t = 0.75$, $p = 0.48$
Chlorpromazine	$-5.41 \pm 1.75(5)^{c}$	$-30.11 \pm 3.32(5)^{b}$	$t = 6.58$, $p < 0.001$

* Significantly differing means are designated by different letters (LSD test, $p < 0.05$).

United States) was placed under the lower part of the body; this allowed control of the anesthetic depth.

The distribution of manganese by mouse brain structures was studied on super-high-field BioSpec 117/16 USR, 11.7 T tomography (Bruker, Germany) by manganese-enhanced MRI (MEMRI) based on T1-weighted images. The Fast Low Angle Shot (FLASH) method using a volumetric RF RES500 1H 089/023 coil (Bruker, Germany) was applied. The parameters of the method include the impulse sequence (TE = 2.5 ms, TR = 200 ms); image parameters (size 2.5 × 2.5 cm; matrix 512 × 512 points); a section thickness of 0.5 mm; and a distance between sections of 0.5 mm. The number of sections was 15. The section orientation is axial, and the total scanning time was 6 min.

The intensity values of T1-weighted images were logarithmed ($\log_2$(MRI signal)) to bring them to a normal distribution. Changes in the MRI signal caused by the introduction of nanoparticles or ions were expressed as a difference between $\log_2$(MRI signal) before and after the introduction of magneto-contrast materials.

Statistical Treatment

The Student's t test was used to compare two mean values; the LSD test was applied for larger number of the means. Data were expressed as means ±SE.

RESULTS

Efficiency of Supply of Magneto-Contrast Compounds from Different OE Regions to Brain

The values of the MRI signal in OB increased depending on the duration of MON exposure in the nasal cavity, which is clearly illustrated by the curves of quantitative estimation of the intensity of T1-weighted images (Fig. 1a). The intensity in the ventral OB already reached the limit values after 20 min exposure of MON in the nasal cavity; this is confirmed by pairwise comparison of MRI signal registered after 20 and 180 min exposure. The difference between these groups was statistically insignificant ($t = 0.53$, $p = 0.61$). At the same time, the accumulation of nanoparticles in the dorsal OB occurred more slowly, and the MRI signal level during nasal cavity washing was statistically significantly lower than during washing after 180 min ($t = 3.43$, $p = 0.009$). The intensity of T1-weighted images did not differ from the maximal values (observed in 180 min of exposure) in only 40 min of exposure ($t = 0.92$, $p = 0.38$).

Different rates of MON accumulation in the ventral and dorsal OB resulted in the fact that the ratio of MRI signals in these regions was higher for all intervals of colloid solution exposure (except for 180 min) as compared with the control group. The maximal ratio of signals in the dorsal and ventral OB took place at a 10-min content of MON in the nasal cavity; it then decreased but exceeded one (up to 180 min) (Fig. 1b). These quantitative differences are clearly illustrated by the examples of tomography images. The MRI signal intensity in the ventral OB significantly exceeded those in the dorsolateral OB with 20 min of MON exposure in the OE (Figs. 1c and 1d).

Unlike nanoparticles, the efficiency of the manganese ion supply in the ventral and dorsal regions OB was almost the same. This is reflected well by the ratio of MRI signal intensity in these regions (MRI_{VOB}/MRI_{DOB}), which did not differ significantly from one (1.07 ± 0.04) ($p > 0.05$). Upon MON application with subsequent washing after 20 min, the signal ratio reached the value of 1.39 ± 0.06 and significantly exceeded those for $MnCl_2$ ($t = 4.44$, $p < 0.001$, Fig. 2).

Effect of Inhibitors of Cellular Transport and Endocytosis on MON Accumulation in OB

The intranasal introduction of colchicines (preceding the application of nanoparticles) suppressed the accumulation of MON in OB (Fig. 3). The MRI signal level in the dorsal OB differed little from the basal level, i.e., from the level registered before the introduction of nanoparticles (0.0001 ± 0.016 and 0.051 ± 0.022, respectively, $t = 1.81$, $p = 0.11$). At the same time, a statistically significant increase in basal values persisted in the ventral OB. In this structure, logarithmed MRI contrast values were 0.130 ± 0.034 upon the introduction of colchicine and MON and 0.0001 ± 0.023 without the introduction of nanoparticles ($t = 3.04$, $p = 0.016$).

A less pronounced, but statistically significant, decrease in the intensity of MRI signal in T1-weighted images in both OB regions was registered upon the introduction of saccharose (nonspecific endocytosis inhibitor) (Fig. 3). The introduction of chlorproma-

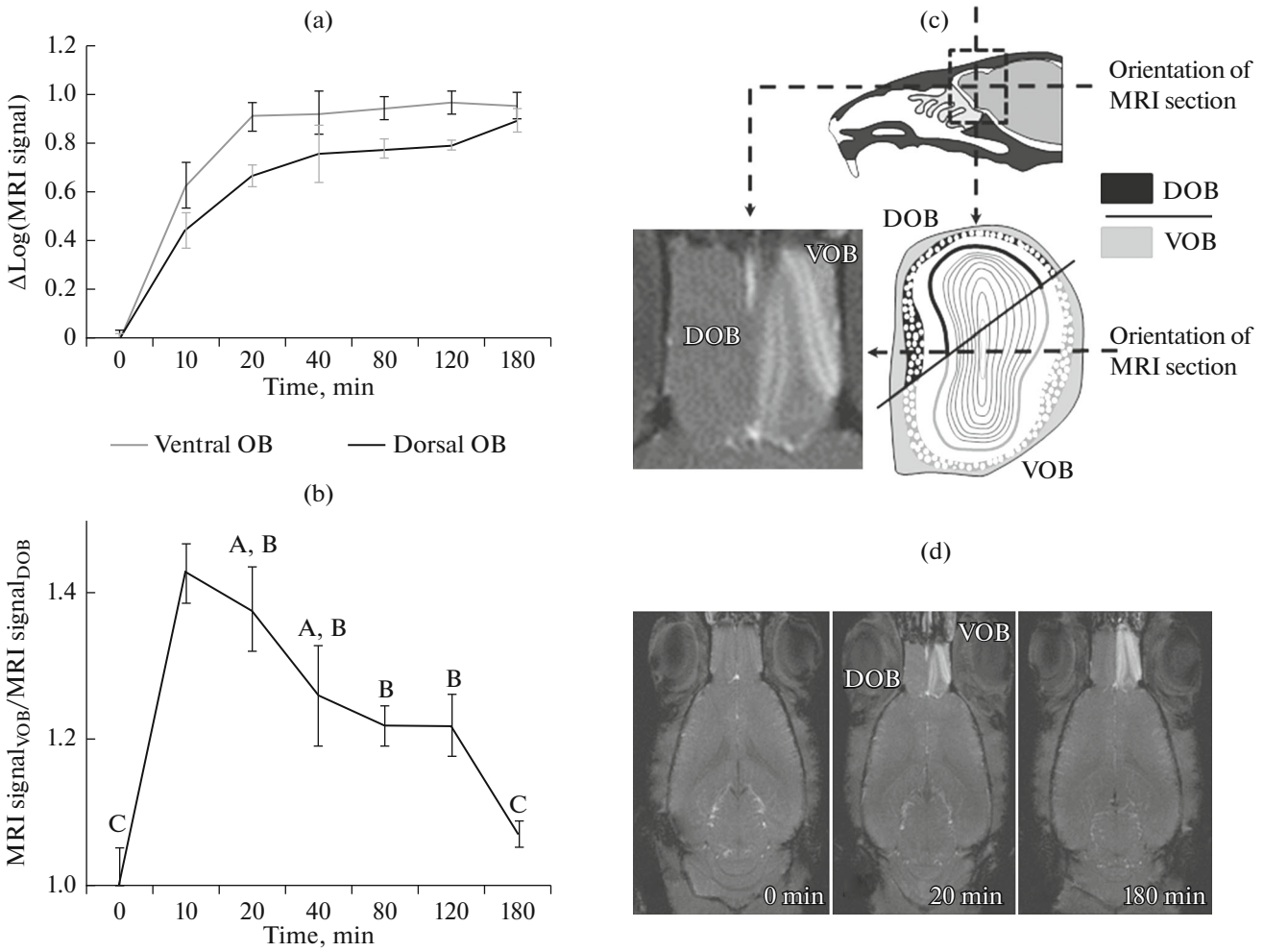

Fig. 1. Changes in MRI contrast as an indicator of the accumulation of nanoparticles in the ventral and dorsal OB upon different exposures of colloid MON solutions in the nasal cavity. (a) Dynamics of MRI signal growth relative to basal values in the ventral and dorsal OB. The horizontal axis (here and in Fig. 1b) shows the time interval from instillation to washing of the nasal cavity. On the ordinate axis, $\Delta\log_2$(MRI signal) = $\log_2$(MRI signal) after MON application – $\log_2$(MRI signal) before MON application. (b) Ratio of MRI signal in the ventral OB to the MRI signal in the dorsal OB. The ordinate axis shows $\Delta\log_2$(MRI signal) in the ventral OB/$\Delta\log_2$(MRI signal) in the dorsal OB. Note: significantly differing mean values ($p < 0.05$, LSD test) are designated by different letters. (c) Sagittal section of mouse head (on which section orientation for OB tomography is demonstrated) is shown at top. T1-weighted MRI image of OB is given at bottom left; the division of the OB according to the projections of dorsal and ventral OE regions on dorsal OB (DOB) and ventral OB (VOB) is shown at the bottom right. (d) Examples of T1-weighted MRI images of OB at 0.20 and 180 min exposures of colloid MON solutions in nasal cavity. DOB and VOB regions are demonstrated by arrows.

zine, which specifically blocks clathrin-dependent endocytosis, resulted in a decreased MRI signal only in the dorsal OB (Fig. 3).

The intensity of the MRI signal in the control group of mice (without the introduction of inhibitors) statistically significantly differed between the ventral OB (1.141 ± 0.034) and dorsal OB (1.026 ± 0.028, $t = 2.50$, $p = 0.037$). Therefore, changes in MRI signal relative to the level registered upon the application of MON without inhibitors were analyzed for careful comparison of inhibiting effects in different OB regions (Table 1). The largest decrease in the intensity of T1-weighted images (equally pronounced in both OB regions) was registered during the introduction of colchicine.

Saccharose had a weaker effect than colchicine. The effect was also the same for the ventral and dorsal OB. The introduction of chlorpromazine in the nasal cavity 5 min before intranasal MON application had no effect on the value of MRI signal in the ventral OB but caused a statistically significant signal decrease in the dorsal OB. The difference in the inhibiting effect value in the compared OB regions was highly significant ($p < 0.001$).

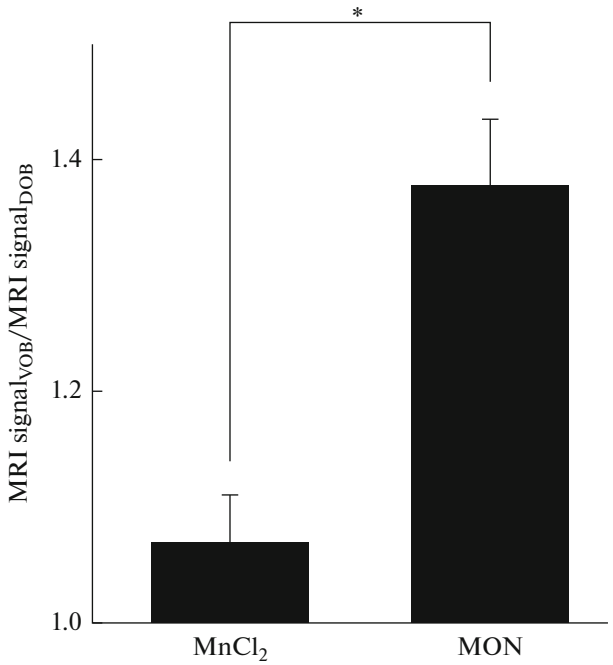

Fig. 2. Ratio of MRI signal values in the ventral OB (VOB) and dorsal OB (DOB) 12 h after 20-min exposure of MON and $MnCl_2$ in the nasal cavity. * $p < 0.001$.

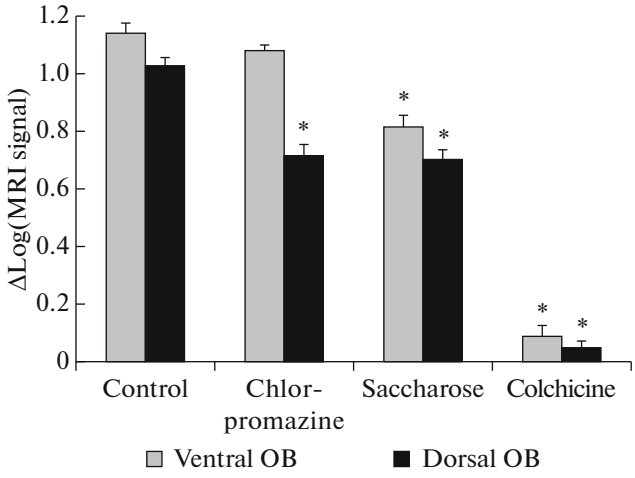

Fig. 3. Effect of inhibitors of endocytosis and cellular transport in MRI signal values ($\Delta\log_2$(MRI signal)) in the ventral and dorsal OB. * Differences from the control level are statistically significant (according to Student's t criterion, $p < 0.05$).

DISCUSSION

The presence of manganese in the brain tissues is manifested in an increased signal on T1-weighted MRI images, the values of which directly depends on manganese concentration in the tissue (Lin and Koretsky, 1997). In particular, microelement analysis of OBs isolated in mice immediately after MRI study demonstrated a correlation coefficient close to one ($r = 0.96$, $p < 0.0001$) between the intensity of tomography signal and Mn content in the tissue (Moshkin et al., 2014). All of this gives grounds to consider the values of the MRI signal a semiquantitative indicator of saturation of the brain tissues with manganese.

By means of MON and manganese-enhanced MRI, we were able to study the dynamics of the capture of solid particles by the ends of olfactory nerves. Nasal cavity washing at different time intervals demonstrated that the majority of MON is captured 20–40 min after intranasal application. An increase in the exposure time to 180 min provides little increase in the signal intensity on T1-weighter tomography images of OB. The introduction of 8–10 μL of colloid MON solution provided a complete filling of the mouse nasal cavity, the volume of which is no more than 8–9 μL (Moshkin et al., 2014). In other words, the conditions of maximal filling of different nasal cavity regions by the solution of nanoparticles were created in our experiments. Nevertheless, the movement of nanoparticles according to the projections of olfactory nerves was more intensive in the ventral region than in the dorsal. As mentioned above, nanoparticles can enter the brain either by diffusion in paracellular space or supply to the blood vessels or by transport and capture within olfactory nerves (Dhuria et al., 2010). In the case of outside axonal transport of MON, it is difficult to expect such a clear linking of magnetic contrast distributions to the morphological organization of the olfactory system (since this took place on T1-weighted OB images). In addition, the introduction of colchicine, which inhibits endocytosis and axonal transport (Ribak et al., 1978) almost completely excluded the accumulation of MRI contrast in olfactory bulbs. This result is further evidence in favor of axonal transport. With its suppression, nanoparticle movement by diffusion in paracellular space, as well as by the blood and lymphatic vessel supply, remains possible; however, the efficiency of these pathways is extremely low.

Intranasal introduction of saccharose (nonspecific endocytosis inhibitor) equally decreased the positive contrast value in ventral OB regions. But chlorpromazine, which specifically suppresses clathrin-dependent endocytosis (Wang et al., 1993), decreased the intensity of MRI signal only in the dorsal OB; this indicates a significant contribution of this mechanism in the capture of nanoparticles on the surface of the appropriate OE region.

The significance of endocytosis as a key cause of different transport efficiency of the dorsal and ventral OE regions supports the experiment with intranasal $MnCl_2$ application, giving manganese and chlorine ions during dissociation. Since Mn^{2+} is close to Ca^{2+}

by its physical–chemical characteristics, the supply of manganese ions from the mucosal OE layer in olfactory neurons is realized through calcium channels (Lin and Koretsky, 1997); according to our data (Fig. 3), this mechanism works with the same efficiency in dorsal and ventral OE regions.

The zonal organization of the olfactory system is provided not only by peculiarities of the expression of olfactory receptor genes but also by the nasal passage geometry, where receptors to the most muco-soluble compounds are concentrated in the region with maximal rate of air flow (dorsal part), while receptors to less volatile compounds are concentrated in the ventral part of the nose (Mori et al., 2000; Scott et al., 2014). The ratio of air flow rates during inspiration between dorsal and ventral methanuses of the nasal cavity varies in different mammalian species: human, 1 : 1 (Zhang and Kleinsteuer, 2004); rat and mouse, 1 : 1.5 (Minard et al., 2006; Moshkin et al., 2014); and dog, 1 : 3 (Craven et al., 2010). An increase in the flow rate in selected areas of nasal cavity makes it possible to increase locally the odor stimulus concentration, increasing the sensitivity to this compound (Scott et al., 2014; Oka et al., 2009). Thus, the largest response to chemical compounds in mice associated with such vitally significant stimuli as the odor of a predator, spoiled food (Kobayakawa et al., 2007), "dirty" litter (Bolon et al., 1991), and a number of others is observed exactly in the dorsal part of olfactory epithelium. The olfactory cells of the dorsal part of nasal cavity innervate the appropriate part of OB, and the receptor cells of the ventral part of nasal cavity innervate the ventral part of the OB, thus translating the geometry of nasal passages on the structures of primary processing of the olfactory information (Schoenfeld and Cleland, 2006).

Since the air flow rate in the dorsal part of the nasal cavity is higher than in the ventral, the introduction of inhaled MON leads to an uneven precipitation of particles in these areas; therefore, the colloid solution of MON in our experiments was introduced intranasally, which allowed leveling of the effect of the nose geometry on particle accumulation in a given part of it. A decrease in MON passage in the dorsal part of the olfactory bulb during their joint presentation with chlorpromazine indicates that clathrin-dependent endocytosis plays a leading role in the capture of nanoparticles by the cells of the dorsal part of the nasal cavity. The absence of significant changes in MON accumulation in the ventral part of the OB during preliminary presentation of chlorpromazine means that MON capture by cells of ventral part of OE is performed due to clathrin-independent endocytosis (for example, due to caveolin-dependent endocytosis or lipid rafts).

Thus, the results of our studies demonstrated that structural and functional organization of the mouse nasal cavity completely meet the adaptive congruence principle, which limits infectious and toxic effects of nanoaerosols on the olfactory cell epithelium and the brain. At present, it is difficult to determine how much this principle is applicable to nose constructions in the animals inhabiting different ecological niches. To answer this question, a comparative study of the geometry of nasal cavities, the activity of detoxifying OE systems, and the efficiency of nasal transport efficiency in different OB regions is required.

ACKNOWLEDGEMENTS

The experimental part of the study and the analysis of the results were supported by the Russian Science Foundation (project no. 14-14-00221). The acquisition of laboratory animals and the use of instrumental resources were provided by the funds of the State Task (project no. 0324-2015-0004).

REFERENCES

Bolon, B., Bonnefoi, M.S., Roberts, K.C., Marshall, M.W., and Morgan, K.T., Toxic interactions in the rat nose: pollutants from soiled bedding and methyl bromide, *Toxicol. Pathol.*, 1991, vol. 19, no. 4 (2), pp. 571–579.

Boucrot, E., Ferreira, A.P., Almeida-Souza, L., Debard, S., and Vallis, Y., Endophilin marks and controls a clathrin-independent endocytic pathway, *Nature*, 2015, vol. 517, no. 7535, pp. 460–465.

Calderón-Garcidueñas, L., Franco-Lira, M., Mora-Tiscareño, A., Medina-Cortina, H., Torres-Jardón, R., and Kavanaugh, M., Early Alzheimer's and Parkinson's disease pathology in urban children: friend versus foe responses—it is time to face the evidence, *BioMed. Res. Int.*, 2013. doi 10.1155/2013/161687

Castel, M.N., Retrograde axonal transport of neurotensin in the dopaminergic nigrostriatal pathway in the rat, *Neuroscience*, 1990, vol. 36, no. 2, pp. 425–430.

Chattopadhyay, S., Dash, S.K., Tripathy, S., Das, B., Mandal, D., Pramanik, P., and Roy, S., Toxicity of cobalt oxide nanoparticles to normal cells; an in vitro and in vivo study, *Chem. Biol. Interact.*, 2015, vol. 226, pp. 58–71.

Craven, B.A., Paterson, E.G., and Settles, G.S., The fluid dynamics of canine olfaction: unique nasal airflow patterns as an explanation of macrosmia, *J. R. Soc. Interface*, 2010, vol. 7, no. 47, pp. 933–943.

Dando, S.J., Mackay-Sim, A., Norton, R., Currie, B.J., John, J.A. St., Ekberg, J.A.K., Batzloff, M., Ulett, G.C., and Beacham, I.R., Pathogens penetrating the central nervous system: infection pathways and the cellular and molecular mechanisms of invasion, *Clin. Microbiol. Rev.*, 2014, vol. 27, no. 4, pp. 691–726.

Dhuria, S.V., Hanson, L.R., and Frey, W.H., Intranasal delivery to the central nervous system: mechanisms and

experimental consideration, *J. Pharm. Sci.*, 2010, vol. 99, no. 4, pp. 1654–1673.

Elder, A., Gelein, R., Silva, V., Feikert, T., Opanashuk, L., Carter, J., Potter, R., Maynard, A., Ito, Y., Finkelstein, J., and Oberdörster, G., Translocation of inhaled ultrafine manganese oxide particles to the central nervous system, *Environ. Health Perspect.*, 2006, vol. 114, no. 8, pp. 1172–1178.

Faber, H.K., Silverberg, R.J., and Dong, L., Poliomyelitis in the cynomolgus monkey. III. Infection by inhalation of droplet nuclei and the nasopharyngeal portal of entry, with a note on this mode of infection in rhesus, *J. Exp. Med.*, 1944, vol. 80, no. 1, pp. 39–57.

Garcia, G.J. and Kimbell, J.S., Deposition of inhaled nanoparticles in the rat nasal passages: dose to the olfactory region, *Inhalation Toxicol.*, 2009, vol. 21, no. 14, pp. 1165–1175.

Garcia, G.J.M., Schroeter, J.D., and Kimbell, J.S., Olfactory deposition of inhaled nanoparticles in humans, *Inhalation Toxicol.*, 2015, vol. 27, no. 8, pp. 394–403.

Hopkins, L.E., Patchin, E.S., Chiu, P.-L., Brandenberger, C., Smiley-Jewell, S., and Pinkerton, K.E., Nose-to-brain transport of aerosolised quantum dots following acute exposure, *Nanotoxicology*, 2014, vol. 8, no. 8, pp. 885–893.

Hussain, S.M., Javorina, A.K., Schrand, A.M., Duhar, H.M., Ali, S.F., and Schlager, J.J., The interaction of manganese nanoparticles with PC-12 cells induces dopamine depletion, *Toxicol. Sci.*, 2006, vol. 92, no. 2, pp. 456–463.

Jiang, J. and Zhao, K., Airflow and nanoparticle deposition in rat nose under various breathing and sniffing conditions—a computational evaluation of the unsteady and turbulent effect, *J. Aeros. Sci.*, 2010, vol. 41, no. 11, pp. 1030–1043.

John, J.A. St., Ekberg, J.A.K., Dando, S.J., Meedeniya, A.C.B., Horton, R.E., Batzloff, M., Owen, S.J., Holt, S., Peak, I.R., and Ulett, G.C., *Burkholderia pseudomallei* penetrates the brain via destruction of the olfactory and trigeminal nerves: implications for the pathogenesis of neurological melioidosis, *MBio*, 2014, vol. 5, no. 2, pp. 00025–00014.

Kittler, J.T., Delmas, P., Jovanovic, J.N., Brown, D.A., Smart, T.G., and Moss, S.J., Constitutive endocytosis of GABAA receptors by an association with the adaptin AP2 complex modulates inhibitory synaptic currents in hippocampal neurons, *J. Neurosci.*, 2000, vol. 20, no. 21, pp. 7972–7977.

Kobayakawa, K., Kobayakawa, R., Matsumoto, H., Oka, Y., Imai, T., Ikawa, M., Okabe, M., Ikeda, T., Itohara, S., and Kikusui, T., Innate versus learned odor processing in the mouse olfactory bulb, *Nature,* 2007, vol. 450, no. 7169, pp. 503–508.

Lin, Y.J. and Koretsky, A.P., Manganese ion enhances T1-weighted MRI during brain activation: An approach to direct imaging of brain function, *Magn. Reson. Med.*, 1997, vol. 38, no. 3, pp. 378–388.

Minard, K.R., Einstein, D.R., Jacob, R.E., Kabilan, S., Kuprat, A.P., Timchalk, C.A., Trease, L.L., and Corley, R.A., Application of magnetic resonance (MR) imaging for the development and validation of computational fluid dynamic (CFD) models of the rat respiratory system, *Inhalation Toxicol.,* 2006, vol. 18, no. 10, pp. 787–794.

Moore, R.H., Sadovnikoff, N., Hoffenberg, S., Liu, S., Woodford, P., Angelides, K., Trial, J.A., Carsrud, N.D., Dickey, B.F., and Knoll, B.J., Ligand-stimulated beta 2-adrenergic receptor internalization via the constitutive endocytic pathway into rab5-containing endosomes, *J. Cell Sci.*, 1995, vol. 108, no. 9, pp. 2983–2991.

Mori, I., Komatsu, T., Takeuchi, K., Nakakuki, K., Sudo, M., and Kimura, Y., Parainfluenza virus type 1 infects olfactory neurons and establishes long-term persistence in the nerve tissue, *J. Gen. Virol.*, 1995, vol. 76, no. 5, pp. 1251–1254.

Mori, K., von Campenhausen, H., and Yoshihara, Y., Zonal organization of the mammalian main and accessory olfactory systems, *Philos. Trans. R. Soc., B*, 2000, vol. 355, no. 1404, pp. 1801–1812.

Mori, I., Nishiyama, Y., Yokochi, T., and Kimura, Y., Olfactory transmission of neurotropic viruses, *J. Neurovirol.*, 2005, vol. 11, no. 2, pp. 129–137.

Moshkin, M.P., Petrovski, D.V., and Akulov, A.E., Nasal aerodynamics protects brain and lung from inhaled dust in subterranean diggers, *Ellobius talpinus, Philos. Trans. R. Soc., B*, 2014, vol. 281, no. 1792, p. 919.

Moshkin, M.P., Petrovski, D.V., Akulov, A.E., Romaschenko, A.V., Gerlinskaya, L.A., Muchnaya, M.I., Ganimedov, V.L., Sadovsky, A.S., Savelov, A.A., Koptyug, I.V., Troitsky, S.Yu., Bukhtiyarov, V.I., Kolchanov, N.A., Sagdeyev, R.Z., and Fomin, V.M., Aerosol deposition in nasal passages of burrowing and ground rodents when breathing dust-laden air, *Biol. Bull. Rev.*, 2015, vol. 5, no. 1, pp. 36–45.

Munster, V.J., Prescott, J.B., Bushmaker, T., Long, D., Rosenke, R., Thomas, T., Scott, D., Fischer, E.R., Feldmann, H., and de Wit, E., Rapid Nipah virus entry into the central nervous system of hamsters via the olfactory route, *Sci. Rep.*, 2012, vol. 2, no. 2, p. 736. doi 10.1038/srep00736

Oberdörster, G., Sharp, Z., Atudorei, V., Elder, A., Gelein, R., Kreyling, W., and Cox, C., Translocation of inhaled ultrafine particles to the brain, *Inhalation Toxicol.*, 2004, vol. 16, nos. 6–7, pp. 437–445.

Oka, Y., Takai, Y., and Touhara, K., Nasal airflow rate affects the sensitivity and pattern of glomerular odorant responses in the mouse olfactory bulb, *J. Neurosci.,* 2009, vol. 29, no. 39, pp. 12070–12078.

Ribak, C.E., Vaughn, J.E., and Saito, K., Immunocytochemical localization of glutamic acid decarboxylase in neuronal somata following colchicine inhibition of axonal transport, *Brain Res.*, 1978, vol. 140, no. 2, pp. 315–332.

Ryzhikov, A.B., Ryabchikova, E.I., Sergeev, A.N., and Tkacheva, N.V., Spread of Venezuelan equine encephalitis virus in mice olfactory tract, *Arch. Virol.*, 1995, vol. 140, pp. 2243–2254.

Schoenfeld, T.A. and Cleland, T.A., Anatomical contributions to odorant sampling and representation in rodents: zoning in on sniffing behavior, *Chem. Sens.*, 2006, vol. 31, no. 2, pp. 131–144.

Scott, J.W., Sherrill, L., Jiang, J., and Zhao, K., Tuning to odor solubility and sorption pattern in olfactory epithelial responses, *J. Neurosci.*, 2014, vol. 34, no. 6, pp. 2025–2036.

Shi, H., Kleinstreuer, C., and Zhang, Z., Dilute suspension flow with nanoparticle deposition in a representative nasal airway model, *Phys. Fluids*, 2008, vol. 20, no. 013301, pp. 1–23.

Sloot, W.N. and Gramsbergen, J.B.P., Axonal transport of manganese and its relevance to selective neurotoxicity in the rat basal ganglia, *Brain Res.*, 1994, vol. 657, no. 1, pp. 124–132.

Wang, L.-H., Rothberg, K.G., and Anderson, R.G., Misassembly of clathrin lattices on endosomes reveals a regulatory switch for coated pit formation, *J. Cell Biol.*, 1993, vol. 123, no. 5, pp. 1107–1117.

Wang, J.X., Liu, Y., Jiao, F., Lao, F., Li, W., Gu, Y.Q., Li, Y.F., Ge, C.C., Zhou, G.Q., and Li, B., Time-dependent translocation and potential impairment on central nervous system by intranasally instilled TiO_2 nanoparticles, *Toxicology*, 2008, vol. 250, nos. 1–2, pp. 82–90.

Wu, J., Wang, C., Sun, J., and Xue, Y., Neurotoxicity of silica nanoparticles: brain localization and dopaminergic neurons damage pathways, *ACS Nano*, 2011, vol. 5, no. 6, pp. 4476–4489.

Zhang, Z. and Kleinstreuer, C., Airflow structures and nano-particle deposition in a human upper airway model, *J. Comput. Phys.*, 2004, vol. 198, no. 1, pp. 178–210.

Translated by A. Barkhash